

Impact of control signal phase noise on qubit fidelity

Agata Barsotti, Paolo Marconcini, Gregorio Procioli, and Massimo Macucci*

Dipartimento di Ingegneria dell'Informazione, Università di Pisa

Via Caruso 16, I-56122 Pisa, Italy

As qubit decoherence times are increased and readout technologies are improved, nonidealities in the drive signals, such as phase noise, are going to represent a growing limitation to the fidelity achievable at the end of complex control pulse sequences. Here we study the impact on fidelity of phase noise affecting reference oscillators with the help of numerical simulations, which allow us to directly take into account the interaction between the phase fluctuations in the control signals and the evolution of the qubit state.

Our method is based on the generation of phase noise realizations consistent with a given power spectral density, that are then applied to the pulse carrier in simulations, with Qiskit-Dynamics, of the qubit temporal evolution. By comparing the final state obtained at the end of a noisy pulse sequence with that in the ideal case and averaging over multiple noise realizations, we estimate the resulting degradation in fidelity, and exploiting an approximate analytical representation of a carrier affected by phase fluctuations, we discuss the contributions of the different spectral components of phase noise.

INTRODUCTION

Developing large-scale reliable and viable quantum computers is at present one of the main objectives of the scientific community. The physical implementations of the unit of quantum information, the qubit, are characterized by two main parameters, that are fundamental indicators of their performance: the relaxation time T_1 and the coherence time T_2^* [1–4]. Both of these parameters must be optimized, and, in particular, decoherence, the process through which freely evolving qubits gradually lose stored information, represents one of the main limitations. Error mitigation techniques, in particular quantum error correction (QEC) algorithms, have been developed, but their successful implementation requires that qubits have coherence times long enough for the QEC routines to be executed [5–7]. Sources of decoherence are random physical processes in the environment surrounding the quantum processor, but also noise and fluctuations in the signals used to control qubits. Therefore, specifically understanding and reducing the effects of noise on decoherence are fundamental challenges within the overall development of quantum computers.

Here, we focus on the investigation of the action of the noise affecting the pulses used to control qubit evolution, and, in particular, of phase noise, which is the prevalent nonideality (other forms of noise, such as thermal and shot noise, have in general a minor effect in this specific application). We will mainly deal with superconducting qubits, which represent one of the most promising implementations for quantum computers, due to their relatively long coherence times, as well as to the ease of manipulation [8–11].

Over the years, the need to control quantum states with high precision has led to the development of Quantum Control Theory [12–15]. An important aspect of this

theory is the use of spectral overlap techniques to analyze and reduce the effect of environmental noise on control protocols [16, 17]. This approach considers the spectral characteristics of both the noise, through its power spectral density, and of the control pulses or pulse sequences, through the associated filter functions in the Fourier domain. Based on these assumptions, the theory of Dynamical Error Suppression (DES) was developed, which exploits a sequence of appropriately designed pulses to mitigate the effects of dephasing [18–24].

A few years ago, the approach based on filter transfer functions was extended to the analysis of the impact, on the coherence and operational fidelity of qubits, of the phase fluctuations (phase noise) associated to the reference oscillators for control pulse generation. In particular, in Ref. [25] H. Ball et al. extended the usage of the filter function formalism to the study of the effect of the phase fluctuations of the reference clock by shifting such fluctuations onto the qubit. Indeed, the choice of the reference frame is arbitrary, and, therefore, one can assume the local oscillator frame as the reference; thus, phase fluctuations of the local oscillator will appear as opposite phase oscillations of the qubit.

In this work, we instead present a different approach: we consider the rotating frame of the qubit as the reference frame and directly evaluate the interaction between the qubit and the noise present in the control pulses. We also take into account the accumulation of the phase error of the reference clock with respect to the rotating frame. Overall, if correctly applied, the two approaches lead to substantially equivalent results, but we believe that our method makes the investigation of the contribution of each component to fidelity in specific final states easier and more intuitive. Furthermore, we will point out that one of the remarks by Ball et al., namely the asserted relevance of high-frequency phase noise components on qubit infidelity, which has also been picked up by some hardware vendors, ultimately arises from an oversight in their analysis.

Our approach is based on a two-step method: first, we

* Email: massimo.macucci@unipi.it

generate a pseudorandom sequence of phase values distributed in agreement with the assumed (or measured) noise Power Spectral Density (PSD); then, such a sequence is used as an input for a numerical simulation of the evolution in time of the qubit state, performed with Qiskit-Dynamics [26]. The final state reached by the qubit can then be compared with the one from an ideal, noiseless evolution. Simulations are repeated for different realizations of the same phase noise process (changing the seed used to generate the pseudorandom sequence) and averaged to obtain an estimate for the fidelity achievable with each considered choice of noise power spectral density.

RESULTS

We use a two-step approach to quantify the impact of control-pulse phase noise on qubit fidelity. This procedure combines the synthetic phase noise generation with the quantum simulation of the evolution in the time domain performed with Qiskit-Dynamics. The method used to generate sequences of baseband phase noise values for the simulations operates in the discrete-time domain and is based on filtering a white Gaussian process through a Finite Impulse Response (FIR) filter, synthesized on the basis of the desired noise PSD and Impulse Response Truncation (IRT). It will be described in detail in the *Method* section.

Once the baseband phase noise values with specific amplitude and spectral characteristics are obtained, they are used directly as the phase ϕ_j at time t_j of the carrier for the control pulses ($s(t_j) = \Re\{f(t_j) \exp[i(2\pi\nu t_j + \phi_j)]\}$, where $f(t_j)$ is the pulse envelope at t_j , and ν is the carrier frequency), in order to simulate their effect on qubit evolution. In all of our simulations we have considered a rectangular envelope for the control pulses.

We use a sampling frequency of 1 GHz (corresponding to a time step of 1 ns), thus generating a baseband signal limited to a 500 MHz bandwidth, which ensures compliance with the Nyquist criterion. To achieve phase modulation of a 6 GHz carrier, the sampling frequency is subsequently increased by an integer factor through discrete-time resampling. Specifically, the temporal resolution is 1 ns at generation and increases to 83.3 ps after resampling.

We performed the simulations of the qubit time evolution with Qiskit-Dynamics [26], an open-source software which solves the Hamiltonian of the interaction between the electromagnetic field and the qubit. The software numerically integrates the time-dependent Schrödinger equation to compute the evolution of a qubit under the effect of a control Hamiltonian. In our simulations, it allows us to calculate the complete temporal evolution of the qubit state starting from a defined initial condition and driven by control pulses with user-defined parameters. From the solver output, we obtain the temporal evolution of the qubit state vector, which enables us to evaluate the fidelity between the final state and the ideal

state predicted on the basis of the noise-free evolution, thus quantifying the effect of phase noise on the accuracy of qubit control.

Contribution of individual noise spectral components

Our initial objective has been that of understanding the contribution of the different frequency components in the phase noise spectrum around the carrier. We thus considered a phase noise PSD with a Gaussian shape, a bandwidth of 3 kHz and a constant amplitude of -85 dBc/Hz, centered on several frequencies. This allowed us to investigate the impact of the individual phase noise frequency components, varying the center frequencies of the filters while maintaining a constant noise power. The performed tests are based on the previously described approach, with sequences of applied π_x pulses. At the beginning of the first simulation, the qubit state is set to $|0\rangle$ and a sequence of 12 consecutive 50 ns rectangular control pulses, spaced 20 ns apart (implementing 12 consecutive NOT gates) is applied. The amplitude of the pulses is initially tuned to achieve the ideal scenario of near-perfect fidelity, in the absence of noise, i.e., in such a way as to make each 50 ns pulse an ideal π_x -pulse. Finally, the generated phase noise values are applied to the phase of the control pulses. The fidelity of the states resulting after each pulse is then evaluated to quantify the impact of phase noise over time. In Fig. 1, the results of this first simulation are shown, with an average over 20 different realizations for each center frequency. In particular, fidelity values are reported as a function of the frequency offset of each Gaussian PSD from the carrier and of the number of 50 ns π_x -pulses applied. The noise amplitude has been chosen to be unrealistically large, in order to obtain a significant loss of fidelity, so that a reduced number of averages is sufficient to get a good estimate. We observe that the largest contributions to the loss of fidelity occur around the Rabi frequency, which in this case is $1/(2 \cdot 50 \text{ ns}) = 10 \text{ MHz}$.

We have then run other simulations with different choices of the number of pulses, their duration and their separation, in order to better investigate the role of the various parameters. In Fig. 2, the fidelity results for two tests are reported. The data shown in the left panel are for a sequence of 12 pulses 25 ns long, separated by 10 ns intervals, while those in the right panel are for a sequence of 10 pulses 150 ns long, separated by 60 ns intervals. We observe that, as in the previously discussed example, the largest effect on fidelity is due to components close to the Rabi frequencies of the individual experiments, 20 MHz and 3.33 MHz, respectively.

After analyzing the case in which the qubit final state is along the z -axis, we now consider operations involving final states on the equatorial plane of the Bloch sphere (although they cannot be measured directly). In this situation, we have to take into account the fact that the phase of the qubit is always defined relative to the instant-

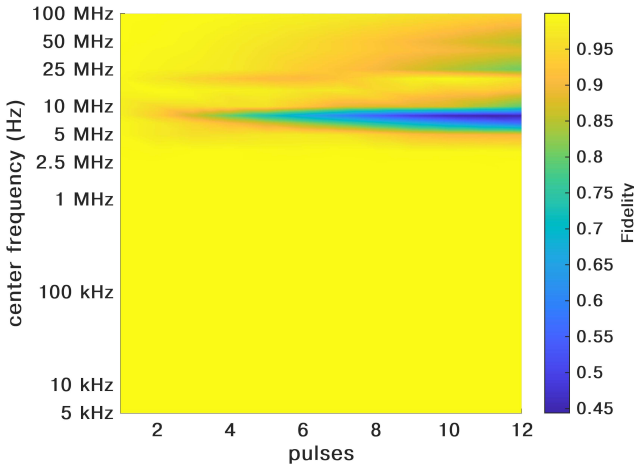


FIG. 1. Fidelity as a function of the frequency offset and of the number of 50 ns π_x -pulses applied with constant amplitudes of -85 dBc/Hz. The qubit is initially prepared in $|0\rangle$

taneous phase of the reference clock used for the control. When no resonant drive is applied, the qubit does not physically interact with the reference clock fluctuations; however, the control reference frame evolves affected by the fluctuations due to phase noise, leading to a relative shift with respect to that of the qubit.

Since fidelity must be evaluated with reference to the control frame (because all subsequent operations will be referred to such a frame), the target state has to be expressed in the same basis. Therefore, for each fidelity evaluation we add the instantaneous reference clock phase deviation to the azimuthal angle of the target state, thus aligning the reference for the evaluation of fidelity with the frame of the local oscillator at the measurement time. This procedure allows us to correctly account for the instantaneous phase deviation of the reference oscillator when evaluating operations on states in the equatorial plane. We then applied the same pulse sequences discussed above, with the same noise power, to a qubit with an initial state on the equatorial plane along the y -axis (Fig. 3), obtaining a somewhat increased degradation of fidelity. This was expected, because of the presence of the additional contribution due to the fluctuations around the z -axis.

As an additional test, we performed the same simulation with a sequence of 12 π_x -pulses of 25 ns duration and the qubit initially prepared in $|0\rangle$, but this time assuming a constant noise amplitude of -95 dBc/Hz, which resulted in a minimum fidelity of 0.9 (Fig. 4).

We have then performed a simulation for a Gaussian shaped phase noise power spectral density with a more realistic bandwidth of 3 MHz (Fig. 5). Except for the bandwidth and the amplitude (which is now -100 dBc/Hz), all the parameters are the same as those for the left panel of Fig. 2. Considering the filter bandwidth, the center frequency of the Gaussian noise spectrum is swept from 10 MHz to 100 MHz. It is apparent that, once again, the maximum effect is close to the Rabi frequency and that

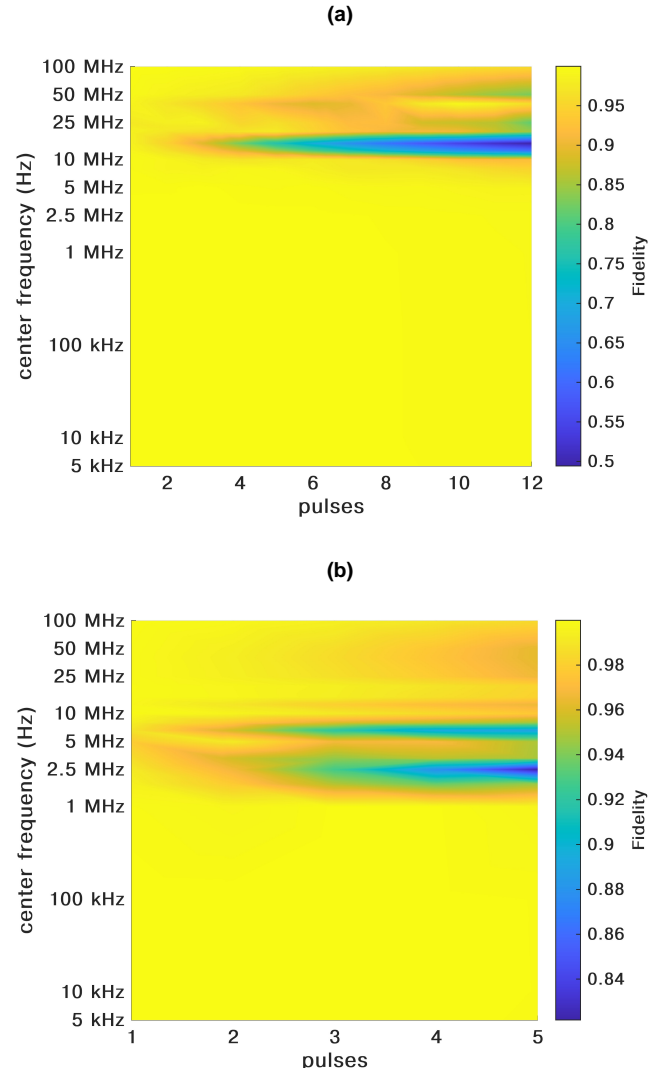


FIG. 2. Fidelity as a function of the number of applied π_x -pulses, with constant amplitudes of -85 dBc/Hz, and of the central frequency of the Gaussian filter used to model phase noise. In both panels the state of the qubit is initially prepared in $|0\rangle$. The top panel (a) shows the results for a sequence of 25 ns pulses separated by 10 ns, while the bottom panel (b) refers to 150 ns pulses with an inter-pulse interval of 60 ns.

high frequency components of the noise spectrum have a reduced effect (which in practice becomes negligible because in the case of a realistic oscillator they have a much lower amplitude with respect to the low frequency components, as discussed in the following). The noise power level has been lowered with respect to the previous case, because otherwise the total noise power associated with the Gaussian spectrum would be much larger (due to the increased bandwidth), leading to an extremely low fidelity.

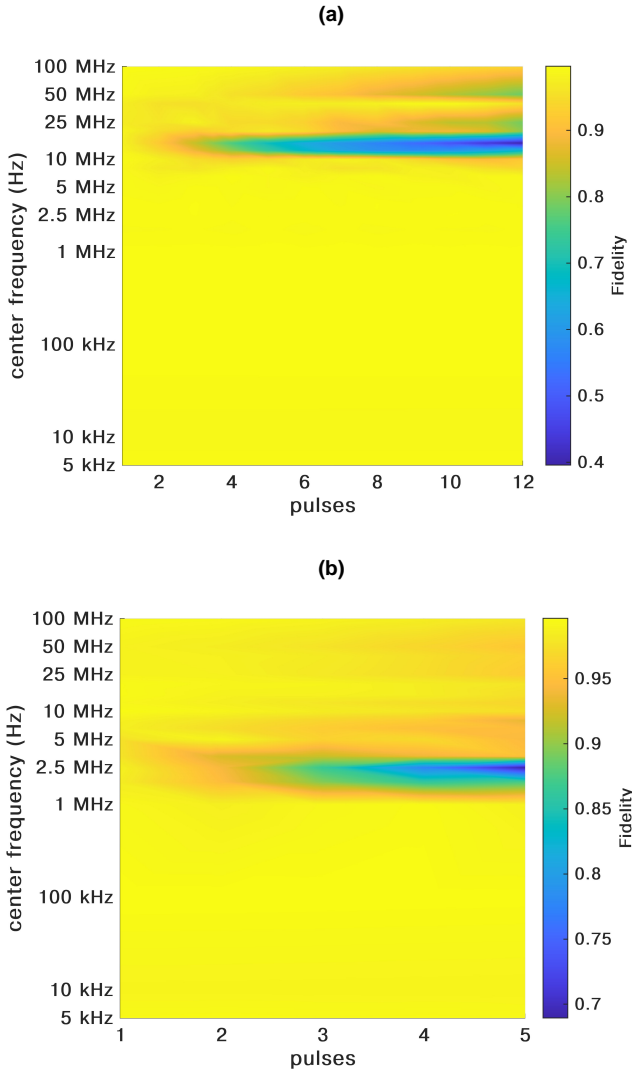


FIG. 3. Fidelity as a function of the number of applied π_x -pulses, with constant amplitudes of -85 dBc/Hz, and of the central frequency of the Gaussian filter used to model phase noise. In both panels the qubit is initially prepared on the equatorial plane of the Bloch sphere, along the y -axis. The top panel (a) shows the results for a sequence of 25 ns pulses separated by 10 ns, while the bottom panel (b) refers to 150 ns pulses with an inter-pulse interval of 60 ns.

Analytical approximation, interpretation and numerical validation

From the results we have presented so far, it is apparent that the largest contribution of phase noise to the loss of fidelity is from frequency components that are at an offset, relative to the qubit resonant frequency, close to the Rabi frequency, which is intuitively reasonable, because the period of the Rabi frequency is the basic timescale of qubit evolution.

On the other hand, it is less intuitively clear why components with high frequency displacement with respect to the resonant frequency could affect the qubit evolution at all, since the qubit, which is intrinsically a resonator,

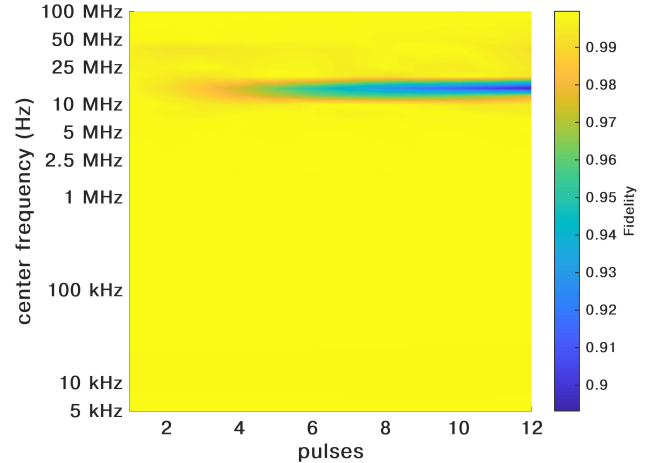


FIG. 4. Fidelity as a function of frequency offset and of the number of 25 ns π_x -pulses applied with a constant amplitudes of -95 dBc/Hz. The qubit is initially prepared in $|0\rangle$

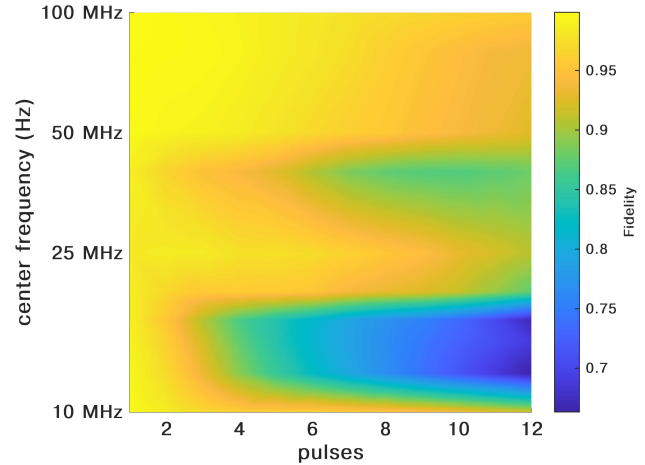


FIG. 5. Fidelity as a function of the frequency offset and of the number of 25 ns π_x -pulses applied with a constant amplitude of -100 dBc/Hz and a bandwidth of the Gaussian FIR filter of 3 MHz. The qubit is initially prepared in $|0\rangle$

should be substantially insensitive to them. In the following, we will discuss this aspect in detail.

Since the level of phase noise affecting the reference clock of the qubit control equipment is usually very low, modulation of the carrier by phase noise can be approximated, up to second order in $\theta(t)$, as:

$$\begin{aligned} \cos[\omega_0 t + \theta(t)] &= \cos(\omega_0 t) \cos[\theta(t)] - \sin(\omega_0 t) \sin[\theta(t)] \simeq \\ &\simeq \cos(\omega_0 t)[1 - \theta(t)^2/2] - \sin(\omega_0 t)\theta(t), \end{aligned} \quad (1)$$

where ω_0 is the control pulse carrier frequency and $\theta(t)$ is the instantaneous (random) phase deviation. Thus, while from the second term on the right hand side we obtain a double sideband modulation (with suppressed carrier) of the phase noise spectrum around the carrier frequency, from the first term we obtain a residual am-

plitude modulation of the carrier.

Let us initially discuss the contribution of the second term, which leads to a direct translation of the noise spectrum around the carrier: thus, the coupling between a noise spectral component and the qubit is analogous to the coupling between a pure sine control signal with the same displacement with respect to the resonance frequency and the qubit. Such a coupling decreases as displacement increases, until it practically vanishes.

This can be shown with a simple simulation: we have applied to the qubit the 12-pulse sequence previously used to obtain the results in Fig. 1, but in this case in the absence of noise. The outcomes of four tests, each with increasing detuning of the pulse carrier from the resonance frequency, are presented in Fig. 6. As detuning increases, it is apparent that the pulses are progressively less effective in driving the expected state transitions or even any perturbation of the state at all. Specifically, with a detuning of 1 MHz (Fig. 6(a)) state inversion with population transfer is still obtained, while for 10 MHz (Fig. 6(b)) significant coupling to the qubit is still present, but the final state wanders around the Bloch sphere. However, with a 50 MHz detuning (Fig. 6(c)), coupling is significantly reduced, with oscillations mainly due to precession around the z -axis. Finally, with a 400 MHz detuning, the initial state is completely preserved, because coupling vanishes.

High frequency components do, however, provide a nonvanishing contribution via the residual amplitude modulation due to the term $\cos(\omega_0 t)[1 - \theta(t)^2/2]$ in Eq. (1): it involves small fluctuations of the carrier amplitude, which lead to fluctuations in the state rotation angle.

In the case of final states along the z -axis of the Bloch sphere, fidelity is not affected by the phase difference between the reference clock frame and the qubit frame (in such a case azimuthal rotations are irrelevant). Such a difference has, indeed, an effect in the case of a final state on the equatorial plane.

This effect must always be included in the results of our simulations (which focus on the direct interaction between the control field and the qubit) whenever the final state is not aligned with z .

Let us now see a simple example for a state on the equatorial plane, discussing one effect at a time: the effect on the polar angle, mainly resulting from the amplitude modulation by noise of the pulse carrier, the effect on the azimuthal angle of the double side band modulation, and, finally, the additional effect on the azimuthal angle of the instantaneous phase shift between the qubit frame and the local oscillator frame.

We start with a state on the equatorial plane, aligned with the y -axis, and apply π_x pulses causing the rotation around the x -axis: the residual amplitude modulation will act only upon the polar angle, since it is varying the amplitude of the control signal and therefore the overall rotation angle. In Fig. 7, we report the evolution of the polar angle during a sequence of 12 π -pulses with a duration of 25 ns (and a separation between pulses of 10 ns)

for a qubit initial state along the negative y -axis. In this case, we generated phase noise sequences through a Gaussian FIR filter with varying center frequencies and a bandwidth of 6 MHz. At the lower frequencies, which are close or relatively close to the Rabi frequency (20 MHz), we observe significant effects due to coupling between the phase noise signal and the qubit (second term in the right hand side of Eq. (1)), while at the highest considered frequency (400 MHz) there is a reduced effect, due to the residual amplitude modulation (first term in the right hand side of Eq. (1)). There is an oscillatory behavior because the state oscillates between the negative and the positive y subspace: let us assume that after the first pulse the state has rotated by an angle slightly less than 180 degrees and therefore the polar angle is slightly more than 90 degrees, let us say $90 + \alpha$ degrees, the second pulse will cause a rotation again of slightly less than 180 degrees, which will lead to a polar angle of $90 - \beta$ degrees, with $\beta > \alpha$, and so forth, therefore an oscillatory behavior with growing amplitude will be observed. The reason why the rotation is always slightly less than 180 degrees is that phase noise applied to an in-phase signal determines a partition of the pulse power between the in-phase component and the quadrature component. The in-phase component will always be smaller than the one without noise, as can be deduced from Eq. (1), where $\cos(\omega_0 t)$ is multiplied by $\cos(\theta)$, which is always less than 1. The amplitude growth can in practice be counteracted by slightly increasing the carrier amplitude.

In Fig. 8 we show the behavior of the component of the azimuthal angle directly obtained from the simulations for (a) odd and (b) even pulses. We see that in this case the effect, now mainly due to the quadrature component, decreases as we raise the frequency and get further from the Rabi frequency, until it substantially disappears at 400 MHz.

In Fig. 9 we report a plot of the component of the azimuthal angle due to the instantaneous value of the phase noise in the control signal, for the same pulse sequence as in the case of Fig. 7. Panel (a) is for the odd pulse numbers and panel (b) for the even pulse numbers. The behavior is random because this is just the sequence of the random phase samples plus 90 (odd pulses) or 270 (even pulses) degrees. Contrary to previously discussed effects, this does not exhibit any accumulation in time.

Contribution of realistic and synthetic noise PSDs

In this Section, we apply our numerical technique to the study of the effect of the phase noise due to two different sources: an actual microwave oscillator [27] that we developed for the up- and down-conversion of control pulses and readout signals, and two synthetic microwave sources with a purposely designed noise PSD.

The former simulation has been performed just to verify the expected performance of our qubit control system in terms of maximum achievable fidelity, while the latter simulation has been devised to provide further evidence

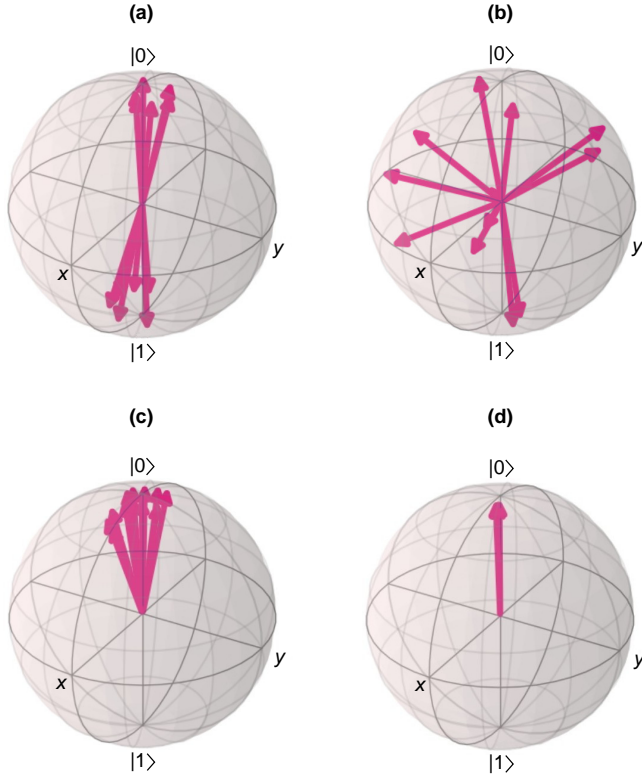


FIG. 6. Bloch sphere representation of a qubit state driven by a pulse with increasing detuning from the resonance frequency. For a detuning of 1 MHz (a), we have transitions of the qubit state from $|1\rangle$ to $|0\rangle$, indicating an efficient population transfer; for a detuning of 10 MHz (b) coupling is still present but the states become scattered all around the Bloch sphere; for a detuning of 50 MHz (c), the state vector mainly precesses around the z -axis; for a detuning of 400 MHz (d), the state vector remains unchanged because coupling is suppressed. This evolution of the polar angle is mainly due to the impact of the amplitude modulation effect.

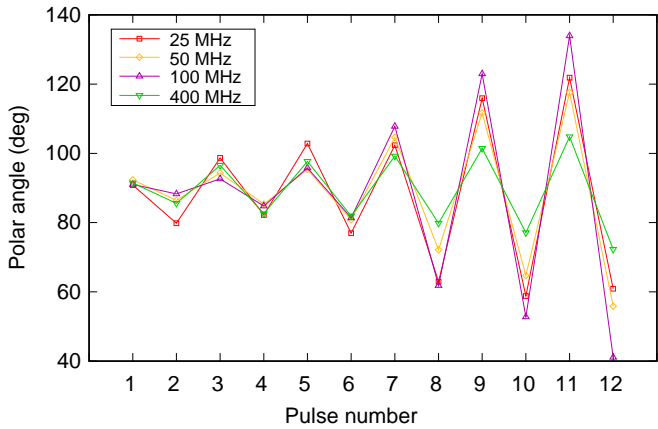


FIG. 7. Evolution of the polar angle. The results correspond to a qubit initially prepared along the negative y -axis and driven by a sequence of twelve 25 ns π_x -pulses, in the presence of phase noise generated through Gaussian FIR filters with different center frequencies and with bandwidth of 6 MHz.

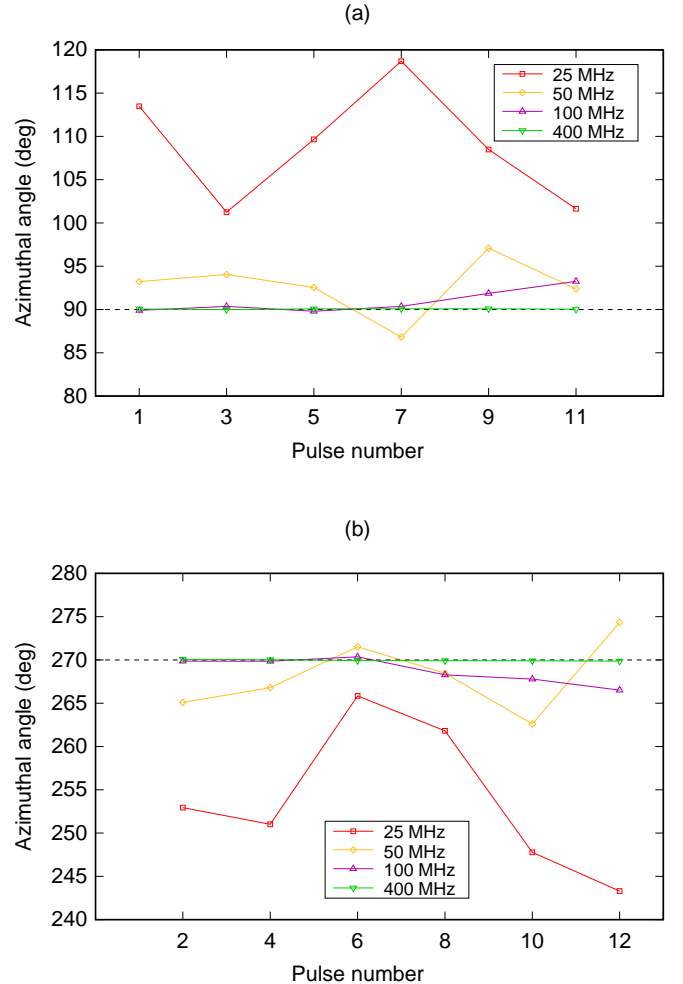


FIG. 8. Evolution of the azimuthal angle, taking into account only the output of the Qiskit-Dynamics simulation (without including the relative phase between the control reference clock frame and the qubit frame). The results are for a qubit initially prepared along the negative y -axis and driven by a sequence of twelve 25 ns π_x -pulses, in the presence of phase noise with Gaussian power spectral densities with different center frequencies and with a bandwidth of 6 MHz.

that the high-frequency components of phase noise do not (as already discussed in the previous sections) have a prevalent effect on fidelity.

We measured the phase noise of an improved version of the oscillator of Ref. [27] with a Rohde & Schwarz FSW spectrum analyzer, and we report the results in Fig. 10, for a carrier at 3.4 GHz. We notice that, while above about 20 kHz the PSD decays with a slope that is approximately $1/f^2$, below 20 kHz we have a peak preceded by a plateau: this is consistent with the action of the phase locked loop, which tends to stabilize the phase of the voltage controlled oscillator (VCO) within the loop bandwidth (assuming that the crystal-based reference oscillator has a lower phase noise compared to the VCO).

The application of phase noise with a PSD equal to that in Fig. 10 to a sequence of ten 150 ns π_x -pulses leads to a very small reduction in fidelity, of the order

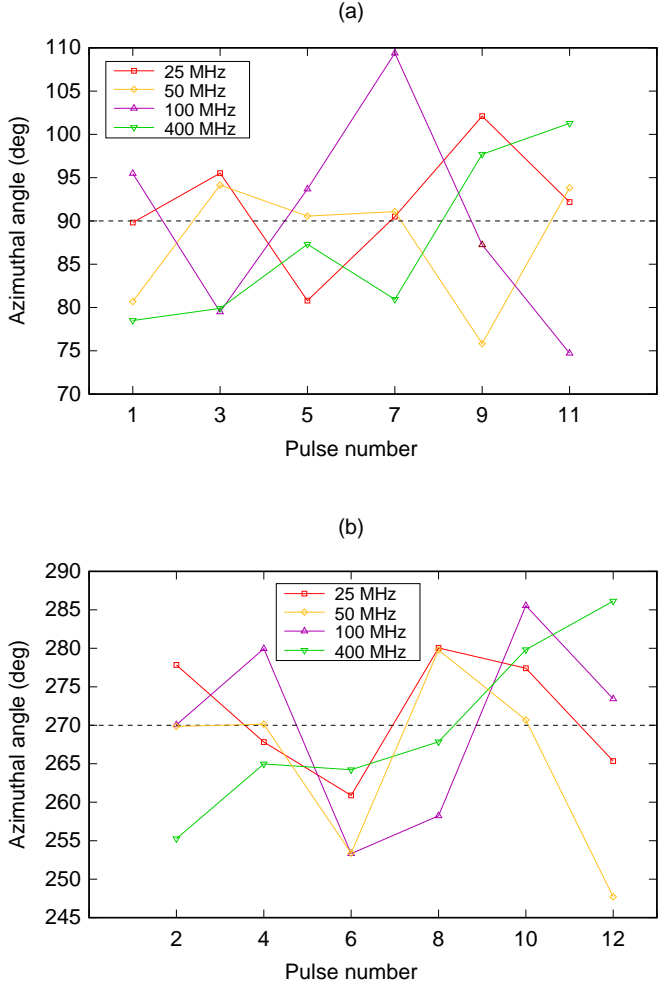


FIG. 9. Evolution of the azimuthal angle, taking into account only the effect of the instantaneous phase deviation of the control signal. The results are for a qubit initially prepared along the negative y -axis and driven by a sequence of twelve 25 ns π_x -pulses, in the presence of phase noise with Gaussian power spectral densities with different center frequencies and with a bandwidth of 6 MHz.

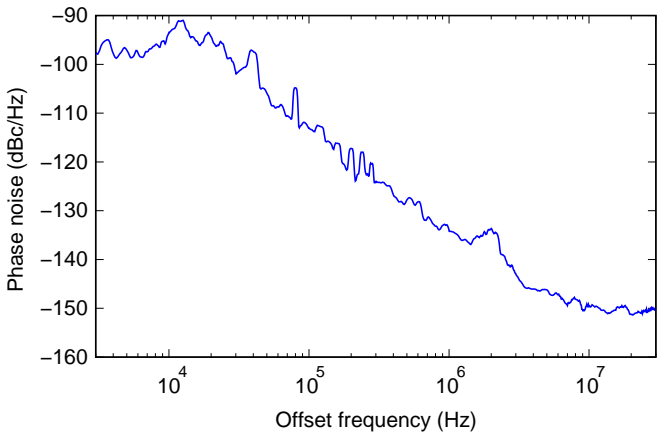


FIG. 10. PSD of the phase noise as a function of the frequency offset for our oscillator for a carrier at 3.4 GHz.

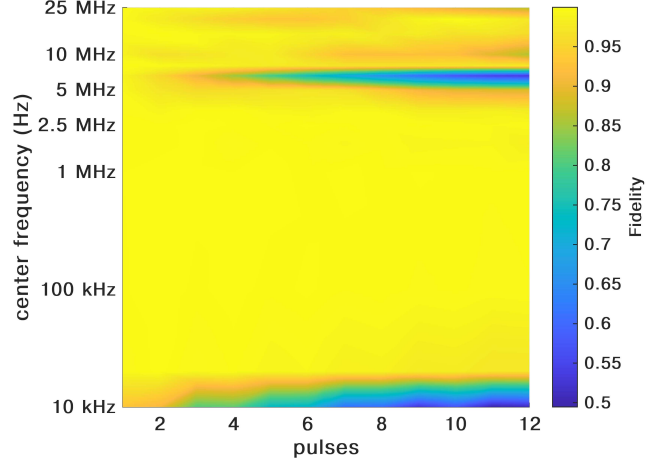


FIG. 11. Fidelity as a function of the frequency offset and of the number of applied 50 ns π_x -pulses, with phase noise amplitudes scaled proportionally to the amplitude of the actual phase noise spectrum of a microwave oscillator (at a 10 MHz offset reaches the value of -104.82 dBc/Hz, and at 10 kHz peaks at around -49 dBc/Hz).

of 10^{-5} , and therefore close to the numerical accuracy of our method.

In this case the noise components at low displacements from the carrier (and with the largest amplitude) have a small effect because the total duration of the pulse sequence (2 μ s) and therefore the observation time are much shorter than the reciprocal of such frequencies.

In order to better understand the role played by the various frequency components, we ran a simulation analogous to those previously discussed with Gaussian shaped filters. This time, however, we used the data from Fig. 10 to assign relative amplitudes for the FIR filters at the various frequencies.

Since the overall effect on fidelity of the power spectral density of Fig. 10 is almost negligible, we have magnified the action by scaling up the phase noise level, in such a way that the PSD at a 10 MHz offset reaches the value of -104.82 dBc/Hz, and at 10 kHz peaks at around -49 dBc/Hz.

We have considered a sequence of twelve 50 ns π_x -pulses separated by 20 ns intervals. The results are reported in Fig. 11, and, as expected, the components close to the Rabi frequency have a predominant effect. However, there is a significant contribution also at low frequencies, resulting from the very large value of the PSD in this frequency range.

This result is in stark contrast with the comments by Ball *et al.* [25], who instead emphasize the role of the components far from the carrier. Indeed, they discuss the contribution of phase noise to fidelity degradation starting from an apparently misinterpreted consideration about the expression of the Noise Power Spectral Density: they argue that, when converting from the phase noise to the frequency noise power spectral density, one has to multiply by ω^2 , which is in principle correct, but

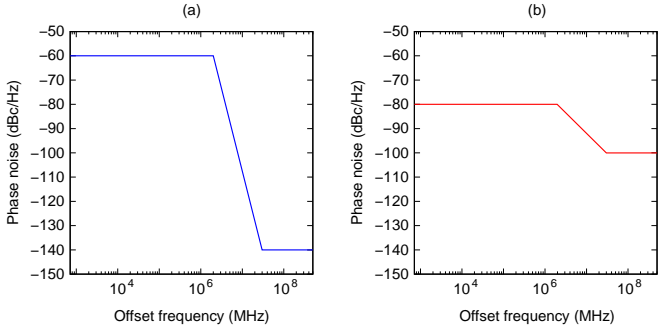


FIG. 12. Synthesized phase noise PSD to study the effect on the fidelity of the frequency components: (a) the noise level is set high at low frequencies (-60 dBc/Hz) and very low at high-frequencies (-140 dBc/Hz); (b) the high-frequency noise components are increased (-100 dBc/Hz) while the low-frequency components are reduced (-80 dBc/Hz).

the frequency noise power spectral density appearing in the expression for the fidelity (Eq. (4) of Ref. [25]) is divided by ω^2 , thus canceling the effect of the previous multiplication. On the basis of the multiplication by ω^2 they state that components of the phase noise spectrum at high frequency, although lower in amplitude, have a stronger effect on fidelity than the much larger low-frequency components. They then proceed to the calculation of the infidelity resulting from the noise from a lab-grade and from a precision local oscillator as a function of the evolution time, also including more complex sequences with dynamical error suppression. We believe that the results of such a calculation are most likely correct, while the argument about the prevalent effect of the high-frequency components in the phase noise of the reference clock is erroneous, for the reason we just mentioned. In order to provide further evidence for our conclusion, we have computed, with our numerical technique, the fidelity achievable for a series of 10 π_x -pulses (each 150 ns long and separated by 60 ns intervals) with a control oscillator affected by two different phase noise spectra, synthesized in such a way as to obtain a situation in which low-frequency noise is strongly prevalent and one in which the low-frequency contribution is decreased and that at high frequency is significantly increased. In particular, we consider the noise spectrum in the left panel of Fig. 12, where the noise level is high at low frequencies, around -60 dBc/Hz up to 2 MHz, and gradually decreases to approximately -140 dBc/Hz for frequencies above 30 MHz. We then consider the spectrum in the right panel, where the PSD is modified by lowering the low-frequency noise plateau by 20 dBc/Hz and raising the high-frequency noise plateau by 40 dBc/Hz. From the results shown in Fig. 13, where the top panel is relative to the noise power spectral density of the left panel of Fig. 12 and the bottom panel is relative to the noise power spectral density of the right panel of Fig. 12, we can therefore conclude that the high-frequency components contribute quite marginally to the loss of fidelity (in particular through residual amplitude modulation, as

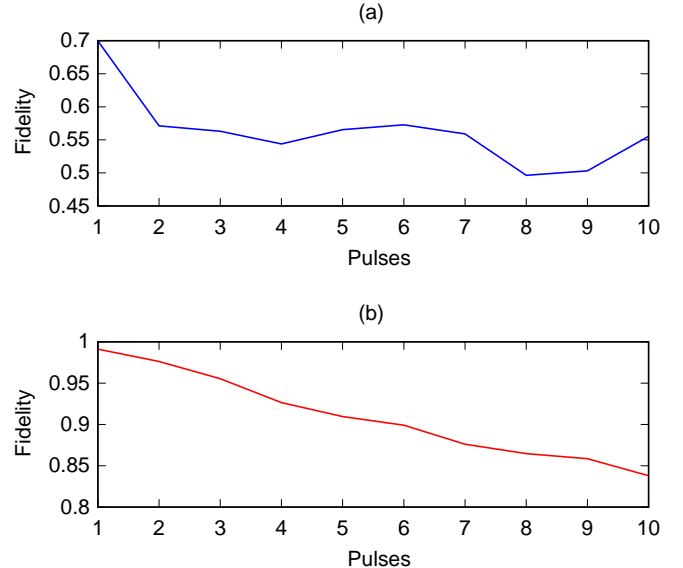


FIG. 13. Fidelity as a function of the number of 150 ns applied π_x -pulses, with the phase noise values from the model described in Fig. 12(a) and Fig. 12(b), respectively.

we have previously discussed).

DISCUSSION

We have investigated the effect of phase noise that affects control signals for superconducting qubits. A numerical method was developed to generate baseband phase noise values with suitable spectral characteristics, which were then added to the instantaneous phase of the carrier for the control pulses used in the simulations. The dynamics of the qubit and the time evolution of the state were simulated with Qiskit-Dynamics, which solves the time-dependent Schrödinger equation for the Hamiltonian describing the interaction between the qubit and the electromagnetic field.

We performed a detailed analysis of the effect of individual frequency components of phase noise on the fidelity of the final states. Starting from the analytical expression of a carrier affected by phase noise, we derived an approximate formulation that allowed us to identify the contributions related to the different types of noise modulation of the carrier. Finally, we extended the analysis by simulating the effect of a real microwave oscillator and of oscillators with a custom PSD designed to exhibit specific spectral characteristics.

From our results, we conclude that the components that contribute most significantly to the degradation of qubit performance, and thus to the reduction in operational fidelity, are the ones with a displacement with respect to the carrier close to the Rabi frequency, and, in the case of realistic phase noise spectra, those at very low displacement, due to their large relative amplitude, which become progressively more important as the duration of the pulse sequence is increased. Instead, noise compo-

nents at high displacement from the carrier give only a minor contribution, mainly limited to the residual amplitude modulation, because of their strongly suppressed power spectral density level.

METHOD

In this section we present more in detail the numerical procedure we used to generate the baseband phase noise sequences. For a desired frequency response $H_d(e^{j\omega})$ on $-\pi \leq \omega < \pi$, the corresponding *ideal* impulse response is:

$$h_d[n] = \frac{1}{2\pi} \int_{-\pi}^{\pi} H_d(e^{j\omega}) e^{j\omega n} d\omega, \quad n \in \mathbb{Z}, \quad (2)$$

which typically extends infinitely in both directions (i.e., it is noncausal and of infinite length). Such a filter cannot be implemented in practice, since only a finite number of coefficients can be stored and computed.

In practice, given a desired (real) amplitude function $A_d(\omega)$, a convenient approximation of the above filter is obtained through the Impulse Response Truncation (IRT) method. We first construct the *generalized linear-phase* spectrum:

$$H_{\text{GLP}}(e^{j\omega}) = A_d(\omega) e^{j\psi_0} e^{-j\omega M/2}, \quad (3)$$

where M is the filter order (thus $M + 1$ coefficients) and ψ_0 is a constant phase offset that determines the type of symmetry: $\psi_0 = 0$ (symmetric impulse response, Types I/II) or $\psi_0 = \pi/2$ (antisymmetric impulse response, Types III/IV).

The corresponding finite-length FIR impulse response is then:

$$h[n] = \begin{cases} \frac{1}{2\pi} \int_{-\pi}^{\pi} A_d(\omega) e^{j\psi_0} e^{-j\omega M/2} e^{j\omega n} d\omega, & n = 0, 1, \dots, M, \\ 0, & \text{otherwise.} \end{cases} \quad (4)$$

This impulse response is obtained by truncating the inverse Fourier transform of the shifted ideal response

$H_{\text{GLP}}(e^{j\omega})$ over the interval $n = 0, 1, \dots, M$. The resulting FIR filter $h[n]$ is *causal* and exhibits *Generalized Linear Phase (GLP)* behavior, with a constant group delay of $M/2$. The constant phase component ψ_0 specifies the corresponding symmetry type of $h[n]$.

In our numerical procedure, we define the amplitude function $A_d(\omega)$ as the square root of the desired noise PSD, set $\psi_0 = 0$, and we choose even values for the order M (Type I filter). This numerical procedure, shown in more detail in Fig. 14, allows us to obtain a phase noise process with the desired PSD, just by modeling the shape of the FIR filter frequency response. To accelerate the computation of the convolution in the time domain between the white Gaussian process and the impulse response of the filter, the Fast Fourier Transform (FFT) is

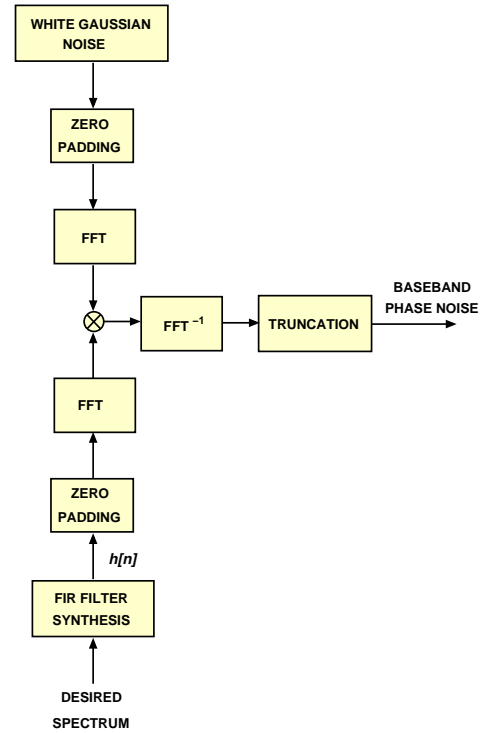


FIG. 14. Block diagram of the numerical procedure to generate baseband phase noise.

leveraged to convert the operation into a multiplication in the frequency domain, performing proper zero-padding to ensure that the vector lengths are powers of 2 [28].

[1] Nielsen, M. A. & Chuang, I. L. *Quantum Computation and Quantum Information: 10th Anniversary Edition* (Cambridge University Press, Cambridge, 2010).
 [2] O’Malley, P. J. J., Kelly, J., Barends, R., Campbell, B., Chen, Y., Chen, Z., Chiaro, B., Dunsworth, A., Fowler, A. G., Hoi, L.-C., Jeffrey, E., Megrant, A., Mutus, J., Neill, C., Quintana, C., Roushan, P., Sank, D., Vainsencher, A., Wenner, J., White, T. C., Korotkov, A., Cleland, A. N. & Martinis, John M. Qubit Metrology of Ultralow Phase Noise Using Randomized Benchmarking. *Phys. Rev. Applied* **3**, 044009 (2015).
 [3] Burnett, J. J., Bengtsson, A., Scigliuzzo, M., Niepce, D., Kudra M., Delsing P. & Bylander J. Decoherence benchmarking of superconducting qubits. *npj Quantum Inf.* **5**, 54 (2019).
 [4] Carroll, M., Rosenblatt, S., Jurcevic, P., Lauer, I. & Kan-

dala, A. Dynamics of superconducting qubit relaxation times. *npj Quantum Inf.* **8**, 132 (2022).

[5] Shor, P. W. Scheme for reducing decoherence in quantum computer memory. *Phys. Rev. A* **52**, R2493(R) (1995).

[6] Ryan-Anderson, C., Bohnet, J. G., Lee, K., Gresh, D., Hankin, A., Gaebler, J. P., Francois, D., Chernoguzov, A., Lucchetti, D., Brown, N. C., Gatterman, T. M., Halit, S. K., Gilmore, K., Gerber, J. A., Neyenhuis, B., Hayes, D. & Stutz, R. P. Realization of real-time fault-tolerant quantum error correction. *Phys. Rev. X* **11**, 041058 (2021).

[7] Caune, L., Skoric, L., Blunt, N. S., Ruban, A., McDaniel, J., Valery, J. A., Patterson, A. D., Gramolin, A. V., Mäjaniemi, J., Barnes, K. M., Bialas, T., Buğdayci, O., Crawford, O., Gehér, G. P., Krovi, H., Matekole, E., Topal, C., Poletto, S., Bryant, M., Snyder, K., Gillespie, N. I., Jones, G., Johar, K., Campbell, E. T. & Hill, A. D. Demonstrating real-time and low-latency quantum error correction with superconducting qubits. Preprint at <https://arxiv.org/abs/2410.05202> (2024).

[8] Krantz, P., Kjaergaard, M., Yan, F., Orlando, T. P., Gustavsson, S. & Oliver, W. D. A quantum engineer's guide to superconducting qubits. *Appl. Phys. Rev.* **6**, 021318 (2019).

[9] Huang, H.-L., Wu, D., Fan, D. & Zhu, X. Superconducting quantum computing: a review. *Sci. China Inf. Sci.* **63**, 180501 (2020).

[10] Gu, X., Kockum, A. F., Miranowicz, A., Liu, Y.-X. & Nori, F. Microwave photonics with superconducting quantum circuits. *Phys. Rep.* **718-719**, 1–102 (2017).

[11] Zhang, E. J., Srinivasan, S., Sundaresan, N., Bogorin, D. F., Martin, Y., Hertzberg, J. B., Timmerwilke, J., Pritchett, E. J., Yau, J.-B., Wang, C., Landers, W., Lewandowski, E. P., Narasgond, A., Rosenblatt, S., Keefe, G. A., Lauer, I., Rothwell, M. B., McClure, D. T., Dial, O. E., Orcutt, J. S., Brink, M. & Chow, J. M. High-performance superconducting quantum processors via laser annealing of transmon qubits. *Sci. Adv.* **8**, eabi6690 (2022).

[12] Huang, G. M., Tarn, T. J. & Clark, John W. On the controllability of quantum-mechanical systems. *J. Math. Phys.* **24**, 2608–2618 (1983).

[13] Viola, L. & Lloyd, S. Dynamical suppression of decoherence in two-state quantum systems. *Phys. Rev. A* **58**, 2733–2744 (1998).

[14] Wiseman, H. M. & Milburn, G. J. *Quantum Measurement and Control* (Cambridge University Press, Cambridge, 2009).

[15] Dong, D. & Petersen, I. R. Quantum control theory and applications: a survey. *IET Control Theory Appl.* **4**, 2651–2671 (2010).

[16] Kofman, A. G. & Kurizki, G. Universal Dynamical Control of Quantum Mechanical Decay: Modulation of the Coupling to the Continuum. *Phys. Rev. Lett.* **87**, 270405 (2001).

[17] Kofman, A. G. & Kurizki, G. Unified Theory of Dynamically Suppressed Qubit Decoherence in Thermal Baths. *Phys. Rev. Lett.* **93**, 130406 (2004).

[18] Viola, L., Knill, E. & Lloyd, S. Dynamical Decoupling of Open Quantum Systems. *Phys. Rev. Lett.* **82**, 2417–2421 (1999).

[19] Uhrig, G. S. Keeping a Quantum Bit Alive by Optimized π-Pulse Sequences. *Phys. Rev. Lett.* **98**, 100504 (2007).

[20] Khodjasteh, K. & Viola, L. Dynamically Error-Corrected Gates for Universal Quantum Computation. *Phys. Rev. Lett.* **102**, 080501 (2009).

[21] Biercuk, M. J., Uys, H., VanDevender, A. P., Shiga, N., Itano, W. M. & Bollinger, J. J. Optimized dynamical decoupling in a model quantum memory. *Nature* **458**, 996–1000 (2009).

[22] Biercuk, M. J., Doherty, A. C. & Uys, H. Dynamical decoupling sequence construction as a filter-design problem. *J. Phys. B: At. Mol. Opt. Phys.* **44**, 154002 (2011).

[23] Green, T., Uys, H. & Biercuk, M. J. High-Order Noise Filtering in Nontrivial Quantum Logic Gates. *Phys. Rev. Lett.* **109**, 020501 (2012).

[24] Green, T. J., Sastrawan, J., Uys, H. & Biercuk, M. J. Arbitrary quantum control of qubits in the presence of universal noise. *New J. Phys.* **15**, 095004 (2013).

[25] Ball, H., Oliver, W. D. & Biercuk, M. J. The role of master clock stability in scalable quantum information processing. *npj Quantum Information* **2**, 16033 (2016).

[26] Puzzuoli, D., Christopher J. W., Daniel J. E., Benjamin, R. & Kento, U. Qiskit Dynamics: A Python package for simulating the time dynamics of quantum systems. *J. Open Source Softw.* **8**, 5853 (2023).

[27] Barsotti, A., Di Pascoli, S. & Macucci, M. Noise Characterization and Optimization in a System for the Measurement of the Coherence Time of Superconducting Qubits. *2024 IEEE International Instrumentation and Measurement Technology Conference (I2MTC)*, 1–6 (2024).

[28] Barsotti, A., Procissi, G., Ciaramelletti, C., Marconcini, P., Guidoni, L., Paganelli, S., & Macucci, M. Effect of Phase Noise in Superconducting Qubit Control. *Lecture Notes in Electrical Engineering* **1263** (Proceedings of SIE 2024), 94–101 (2025).

ACKNOWLEDGEMENT

This work was partially supported by the Italian Ministry of the University and Research (MUR) in the framework of the CrossLab and the FoReLab projects (Departments of Excellence). Financial support is also acknowledged from the European Union, Next-GenerationEU, National Recovery and Resilience Plan (NRRP), Mission 4 Component 2 Investment N. 1.4, CUP N. I53C22000690001, through the National Centre for HPC, Big Data and Quantum Computing (“Spoke 10: Quantum Computing”). This work was supported also by the U.S. Department of Energy, Office of Science, National Quantum Information Science Research Centers, Superconducting Quantum Materials and Systems Center (SQMS), under Contract No. 89243024CSC000002 and by QUART&T, a project funded by the Italian Institute of Nuclear Physics (INFN) within the Technological and Interdisciplinary Research Commission (CSN5)

AUTHOR CONTRIBUTIONS

A.B. wrote the numerical codes, performed the numerical simulations, contributed to the analytical model and collected and processed the output data, G.P. provided the theoretical support for designing the method for the generation baseband phase noise sequences, P.M. contributed to the simulation codes and to processing

the output data. M.M conceived and supervised the project. All authors contributed to the preparation of the manuscript and approved the final version.

COMPETING INTERESTS

All authors declare no competing interests.